Enzyme-Powered Gated Mesoporous Silica Nanomotors for On-Command Intracellular Payload Delivery

Antoni Llopis-Lorente,[abc] Alba García-Fernández,[abc] Nerea Murillo-Cremaes,[d] Ana C. Hortelão,[d] Tania Patiño,[d] Reynadlo Villalonga,[e] Félix Sancenón,[abc] Ramón Martínez-Mañez[abc] and Samuel Sánchez*[df]*

[a] Instituto Interuniversitario de Investigación de Reconocimiento Molecular y Desarrollo Tecnológico (IDM), Universitat Politècnica de València, Universitat de Valencia, Spain.

[b] Unidad Mixta UPV-CIPF de Investigación en Mecanismos de Enfermedades y Nanomedicina, Valencia, Universitat Politècnica de València, Centro de Investigación Príncipe Felipe, València, Spain.

[c] CIBER de Bioingeniería, Biomateriales y Nanomedicina (CIBER-BBN) (Spain).

[d] Institute for Bioengineering of Catalonia (IBEC). The Barcelona Institute of Science and Technology. Baldiri Reixac 10-12, 08028 Barcelona, Spain.

[e] Department of Analytical Chemistry, Faculty of Chemistry, Complutense University of Madrid, 28040, Madrid, Spain.

[f] Institució Catalana de Recerca i Estudies Avançats (ICREA), Pg. Lluís Companys 23, 08010 Barcelona, Spain.

ABSTRACT. The introduction of stimuli-responsive cargo release capabilities on self-propelled micro- and nanomotors holds enormous potential in a number of applications in the biomedical field. Herein we report the preparation of mesoporous silica nanoparticles gated with pH-responsive supramolecular nanovalves and equipped with urease enzymes which act as chemical engines to power the nanomotors. The nanoparticles are loaded with different cargo molecules ($[Ru(bpy)_3]Cl_2$ (bpy=2,2'-bipyridine) or doxorubicin), grafted with benzimidazole groups on the outer surface and capped by the formation of inclusion complexes between benzimidazole and cyclodextrin-modified urease. The nanomotor exhibits enhanced Brownian motion in the presence of urea. Moreover, no cargo is released at neutral pH, even in the presence of the biofuel urea, due to the blockage of the pores by the bulky benzimidazole:cyclodextrin-urease caps. Cargo delivery is only triggered on-command at acidic pH due to the protonation of benzimidazole groups, the dethreading of the supramolecular nanovalves and the subsequent uncapping of the nanoparticles. Experiments in cell culture media indicate that the presence of biofuel (urea) enhances nanoparticle internalization and both, $[Ru(bpy)_3]Cl_2$ or doxorubicin intracellular release, due to the acidity of lysosomal compartments. Gated enzyme-powered nanomotors shown here display some of the requirements for ideal drug delivery carriers such as the capacity to self-propel and the ability to "sense" the environment and deliver the payload on demand in response to predefined stimuli.

Development of micro- and nanobots is an ambitious and multidisciplinary research topic that may lead to revolutionary advancements in different areas such as medicine, sensing and environmental science.[1-5] In the field of drug delivery, the design of advanced nanoparticles able to self-propel in an aqueous environment and to deliver the drug on-command holds great potential to improve classical treatments. Propulsion can be achieved using different approaches such as the

use of light,[6,7] magnetic fields,[8] ultrasounds[9] or by catalysis.[10,11] In recent years, several proof-of-concept studies regarding the use of nanoscale motors in drug delivery have been conducted.[12] Wang and co-workers reported porous gold nanowires of 1.8 μm in length that were propelled by ultrasounds and released doxorubicin around cells upon light irradiation.[13] He's team developed layer-by-layer quitosan-alginate-platinum nanotubes with a length of 8-10 μm that propelled in 3% H_2O_2, attached to the outer surface of HeLa cells and released doxorubicin upon sonication.[14] Additionally, H_2O_2-fueled Janus platinum-mesoporous silica nanomotors loaded with model cargos have also been reported.[15] On the other hand, Wilson's group developed platinum-nanoparticle loaded stomatocytes that propelled by converting H_2O_2 and released doxorubicin upon degradation.[16,17] Notwithstanding, the employment of toxic fuels such as H_2O_2 or hydrazine limits the use of these systems in realistic biological environments.[18,19] In the quest for alternative fuels and catalysts, the use of enzymatic reactions to propel micro- and nanostructures has been regarded as an excellent and versatile alternative[20-22] and several studies have reported autonomous motion of enzyme-driven micro-objects,[23-29] metallic nanorods,[30] nanoparticles,[31,32] and polymeric structures.[33-35]

Another important issue when designing drug delivery systems is the possibility of "reading" information from the environment and deliver the cargo at-will upon the presence or application of a specific stimulus.[36-38] This contrasts with passive delivery systems in which cargo release is achieved by simple diffusion or/and by the slow degradation of the carrier. Among potential nanocarriers, mesoporous silicas are highly appealing since they offer advantageous properties such as easy synthesis, large specific surface area, high loading capacity and biocompatibility.[39] Moreover, the possibility of attaching "molecular gates" (also known as nanovalves or gatekeepers) on the external surface allows designing gated materials that ideally show "zero"

release until an external stimulus is present.[40-42] A wide variety of gated materials able to respond to different stimuli such as light, temperature, magnetic fields, pH, molecules and biomolecules have been developed.[43-48]

Mesoporous silica has already been tested as scaffold for the preparation of enzyme-powered microcapsules,[25] tubular jets,[26] Janus Pt-based motors,[15,49] and enzyme-powered nanoparticles.[31] Recently, light-propelled Janus mesoporous silica nanomotors modified with macrophage cell membrane were showed to percolate into cancer cells.[50] Mesoporous silica-based nanomotors have also been loaded with drugs and presented enhanced diffusion when exposed to fuel, resulting in enhanced drug release kinetics.[32] However, in previously reported examples the pores of mesoporous silica were not gated and a sustained unspecific cargo release was observed, limiting somehow their potential application since a non-negligible amount of drug would be released before reaching a target location. In this scenario, it is apparent from the literature that enzyme-powered gated mesoporous silica nanomotors able to deliver the payload at-will have not yet been developed. In fact, the advantages of combining self-propulsion abilities and stimuli-responsive delivery systems, when compared to passive drug carriers, are immediately obvious; this constitutes the basis of vehicles with a continuous driving force able to "read" information (i.e. the stimulus) from environment and act accordingly, for instance releasing on-demand a certain drug.

Herein, we present the design, preparation and characterization of enzymatic nanomotors based on mesoporous silica gated with pH-responsive supramolecular nanovalves. The design of the nanomotor is depicted in Figure 1. It consists of mesoporous silica nanoparticles, functionalized with benzimidazole groups, loaded with a dye or a model drug (i.e. $[Ru(bpy)_3]Cl_2$ (bpy=2,2'-bipyridine) or doxorubicin) and capped with cyclodextrin-modified urease (CD-U) via the formation of inclusion complexes between CD-U and the benzimidazole moieties. Urease units

allow the enhanced Brownian motion of nanoparticles in the presence of urea as biofuel. At the same time, the benzimidazole:CD-U nanovalves act as bulky caps that prevent cargo release at physiological pH, whereas cargo delivery is observed at acidic pH due to protonation of the benzimidazole groups and the subsequent dethreading of the benzimidazole:CD-U inclusion complexes. Studies with HeLa cells show that the nanomotors enhance internalization in the presence of the urea biofuel and the payload is released upon cellular uptake due to the acidic environment of the lysosomes.

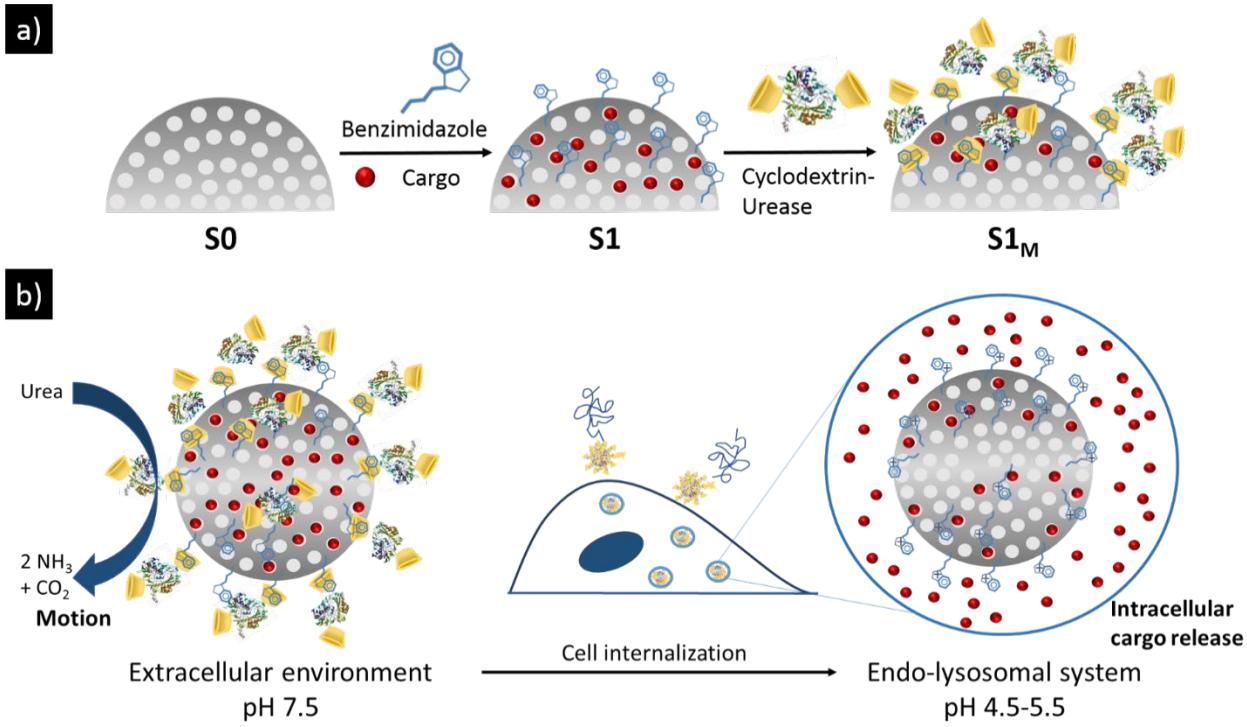

Figure 1. Schematic illustration of the fabrication and performance of enzyme-powered stimuli-responsive nanomotors. a) Schematic of the fabrication process. Nanomotors consist of mesoporous silica nanoparticles loaded with a cargo (a dye or a drug), functionalized with benzimidazole groups on the outer surface and capped with cyclodextrin-modified urease. b) These biocatalytic nanomotors exhibit enhanced Brownian motion due to the enzymatic conversion of urea, and release their cargo at acidic pH through the dethreading of the supramolecular nanovalve.

RESULTS AND DISCUSSION

Nanoparticles synthesis and characterization.

MCM-41 type mesoporous silica nanoparticles were synthesized by hydrolysis and condensation of tetraethyl orthosilicate (TEOS) in aqueous media basified with triethanolamine and using cetyltrimethylammonium bromide (CTAB) as structure-directing agent (see Experimental Section for details). The CTAB surfactant was then removed by acidic extraction in methanol, which yielded the starting mesoporous nanoparticles (**S0**). Then, the process of nanomotor assembly proceeded as schematized in Figure 1a. First, the nanoparticles were suspended in an acetonitrile solution containing the dye $[Ru(bpy)_3]Cl_2$, in order to load the pores by stirring overnight. Next, 3-iodopropyltrimethoxysilane was anchored on the outer silica surface by reaction with silanol groups. In a further step, nucleophilic substitution between the grafted iodopropyl moieties and benzimidazole yielded the benzimidazole-functionalized solid **S1**. Finally, cyclodextrin-modified urease (CD-U) (prepared following a previously reported procedure)[51] was added to an aqueous dispersion of **S1** nanoparticles at pH 7.5 in order to cap the pores via the formation of inclusion complexes between benzimidazole and cyclodextrin groups. The solid was collected by centrifugation and exhaustively washed with phosphate buffer, yielding the final enzyme-powered gated mesoporous silica nanomotors $\mathbf{S1_M}$.

Scanning electron microscopy (SEM) images of **S0** (Figure 2a and Figure SI-1) confirmed the formation of the nanoparticles with good monodispersity in size and a spherical shape. From statistical analysis of SEM images, a diameter of 418 ± 21 nm was determined (total particles analyzed = 200) for the starting mesoporous nanoparticles. Such nanomotor size was selected for allowing reliable motion tracking by optical microscopy, since observation of smaller particles is much more challenging. Notwithstanding, the fabrication of sub-100 nm nanomotors with stimuli-

responsive cargo release is appealing for drug delivery and will be investigated in future works. The powder X-Ray diffraction (PXRD) pattern of **S0** showed the typical (100) reflection peak around 2.3° characteristic of MCM-41 type mesoporous materials (Figure SI-2).[52] The preservation of this characteristic peak in the PXRD pattern of **S1** confirmed that loading and functionalization processes did not damage the 3-D mesoporous structure. Furthermore, from N_2 adsorption-desorption isotherms (Figure 2b), a specific surface area of 1195 $cm^2 \cdot g^{-1}$ for **S0** was calculated by applying the Brunauer-Emmett-Teller (BET)[53] model. Pore diameter and pore volume were found to be as 2.44 nm (Figure SI-3) and 0.80 $cm^3 \cdot g^{-1}$, respectively, by using the Barret-Joyner-Halenda (BJH)[54] model on the adsorption branch of the isotherm. For **S1** nanoparticles, volume of adsorbed N_2 decreased due to the filling of pores with the dye and the specific surface area and pore volume reduced to 392 $cm^2 \cdot g^{-1}$ and 0.26 $cm^3 \cdot g^{-1}$, respectively. We also monitored the fabrication process by zeta potential and hydrodynamic diameter using dynamic light scattering (DLS). Zeta potential changed from -40 mV for **S0** to -10 mV for the benzimidazole-functionalized solid **S1** (Figure 2c). For the final nanomotor **S1M**, the surface charge changed to -50 mV. Urease has an isoelectric point of ca. 5.1 (pH at which the net charge of the protein is zero) and therefore it is negatively charged at neutral pH. Thus, the change in zeta potential to a more negative value is consistent with a successful coordination of the negatively-charged enzyme to the benzimidazole-functionalized silica surface. Moreover, the hydrodynamic diameter increased after each preparation step (445, 468 and 494 nm for **S0**, **S1** and **S1M,** respectively) (Figure SI-4). In all cases, a single population distribution was observed indicating that the particles were not aggregated, even after the functionalization with the benzimidazol groups and capping process with the cyclodextrin-modified urease.

From elemental and thermogravimetric analysis, the content of $[Ru(bpy)_3]Cl_2$ and 1-propyl-1-*H*-benzimidazole on **S1** were determined as 220 mg, which corresponds to 22% of dye loading, and 32 mg per g of nanoparticle, respectively. **S1M** was also characterized by TEM (Figure SI-5). The mesopores were clearly observed, confirming the preservation of the morphology and porous structure in the final **S1M** nanomotor. Additionally, scanning transmission electron microscopy coupled with energy dispersive X-ray spectroscopy (STEM-EDX) mapping of **S1M** clearly indicated the presence of Si and O from the silica matrix, Ru atoms (attributed to the cargo), and S (characteristic of enzymes) (Figure 2d). Finally, the amount of protein on the final nanomotor was quantified according to the Bradford method[55] as 108 mg per g of solid.

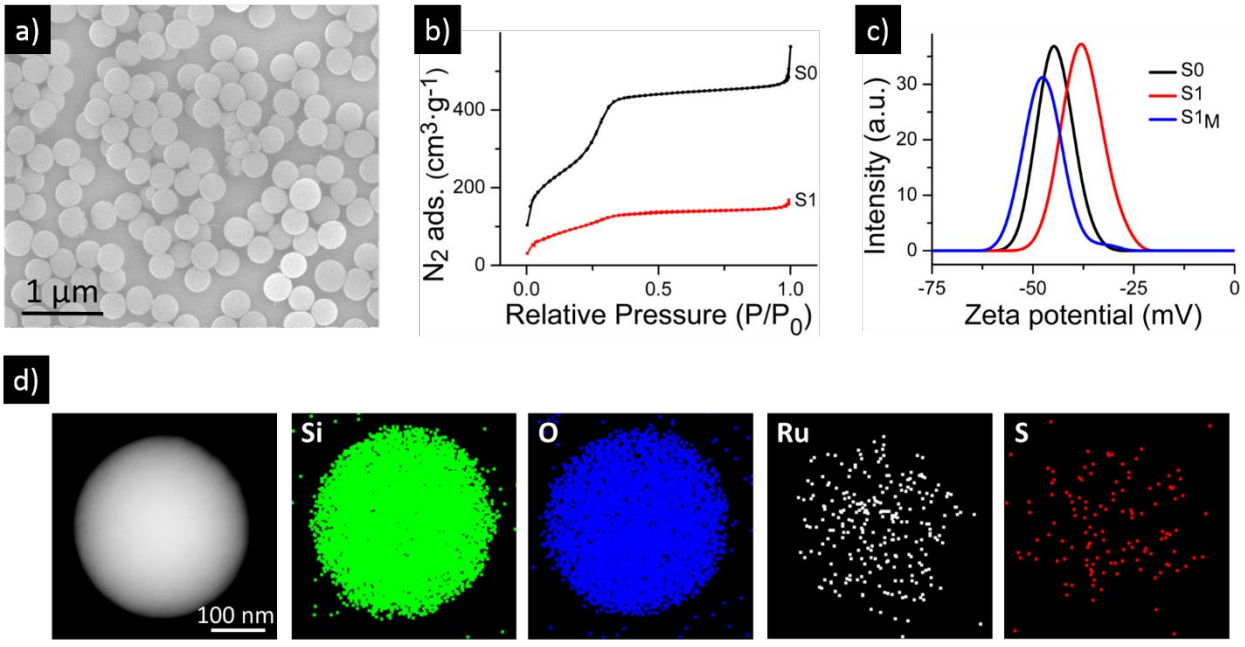

Figure 2. Materials characterization. a) SEM image of the starting mesoporous nanoparticles (**S0**). b) N_2 adsorption-desorption isotherms of **S0** and dye-loaded nanoparticles (**S1**). c) Zeta potential distribution for each preparation step: initial **S0**, loaded and functionalized **S1**, and capped **S1M**. d) STEM-EDX mapping of different atoms for **S1M**: Si and O attributed to the silica scaffold, Ru corresponding to the cargo, and S ascribed to enzymes.

Motion behavior.

In a first step, the catalytic activity of the enzyme-powered gated nanomotors **S1M** was evaluated using a colorimetric urease-specific assay kit based on the Berthelot's method.[56] One unit (U) of urease is defined as the amount of enzyme that catalyzes the hydrolysis of 1 μmol of urea (formation of 2 μmol of ammonia) per minute [i.e. $(NH_2)_2CO + 3H_2O \rightarrow CO_2 + 2NH_4OH$]. In this assay, ammonia produced by the enzymatic process reacts with Berthelot's reagent (alkaline solution of phenol and hypochlorite) to form a blue indophenol product that is measured using a spectrophotometer (λ_{max}=670 nm). A calibration line was obtained from the absorbance of ammonium standards (Figure SI-6), which was used for determining the urease activity on **S1M** as 120 U per gram of nanoparticles (by applying Supplementary Equation 1). This corresponds to 1.1 U per mg of protein (according to the protein quantification by the Bradford assay) and represents a 78% of enzymatic activity compared to the native enzyme.

Once demonstrated the activity of urease on the gated nanomotors **S1M**, motion analysis was performed using optical microscopy. Nanomotors trajectory was tracked in the absence and in the presence of different concentrations of urea in water (see representative trajectories in Figure 3a). From the trajectories, an in-house developed python code was used to compute the mean square displacement (MSD) as a function of time for each condition. MSD always increased linearly with time, which corresponds to typical diffusive motion (Figure SI-7). The resulting MSD was then fitted to MSD = 4 D_e Δt, where D_e represents the effective diffusion coefficient and Δt represents the time interval .[57,58] The diffusion coefficient for **S1M** in the absence of urea (Brownian motion) was found to be 1.06 ± 0.04 $\mu m^2/s$, which is very close to the theoretical value for 418 nm nanoparticles ($D=TK_B/3\pi\eta d$=1.2 $\mu m^2/s$, where T is the temperature, K_B the Boltzmann constant, η the viscosity and d the hydrodynamic diameter). As depicted in Figure 3b, the enzymatic

nanomotors showed a significant increase in the diffusion coefficient dependent on urea concentration, reaching a maximum of 1.47 ± 0.04 $\mu m^2/s$ at 300 mM of urea.

Bearing in mind that a realistic application of the nanomotors should take place in the presence of salts in a physiological media, we evaluated the self-propulsion capabilities in a physiological buffer (PBS, 1X) at different urea concentrations (0, 50, 100 and 300 mM). Representative trajectories in PBS are depicted in Figure SI-8. From the MSD plots (Figure 3c and SI-9), a significant increase in diffusion coefficient from 0.90 ± 0.04 $\mu m^2/s$ (in the absence of urea) to 1.36 ± 0.05 $\mu m^2/s$ (in the presence of 300 mM urea) in PBS was determined (Figure 3d). Despite the decrease in the diffusion coefficients found for **S1M** in PBS (statistically significant with $p<0.02$), the relative increase in the presence of fuel was higher in PBS (48%) than in water (39%), which is in agreement to previously reported urease-powered motors.[32] Additionally, the apparent hydrodynamic diameter determined by DLS decreased in the presence of urea in both media (Figure 3e). Smaller hydrodynamic diameter (*d*) in the presence of fuel correlates with a higher diffusion coefficient (D), according to the Stokes-Einstein equation ($D=TK_B/3\pi\eta d$), thus confirming the enhanced diffusion observed by optical microscopy. Although we are aware that the nanomotor enhanced diffusion may become negligible in the blood flow, we believe that enhanced diffusion can be advantageous in certain tissues or organs (e.g. in tumour tissues or in the bladder) were enhanced diffusion may increment internalization in cells (*vide infra*). Regarding the mechanism of motion of enzymatic motors, a recent study has demonstrated by stochastically optical reconstruction microscopy (STORM) that enzyme molecules are non-homogeneously distributed onto the surface of non-Janus spherical micromotors,[29] which explains the self-propulsion observed in non-Janus spherical particles.[20,29,32]

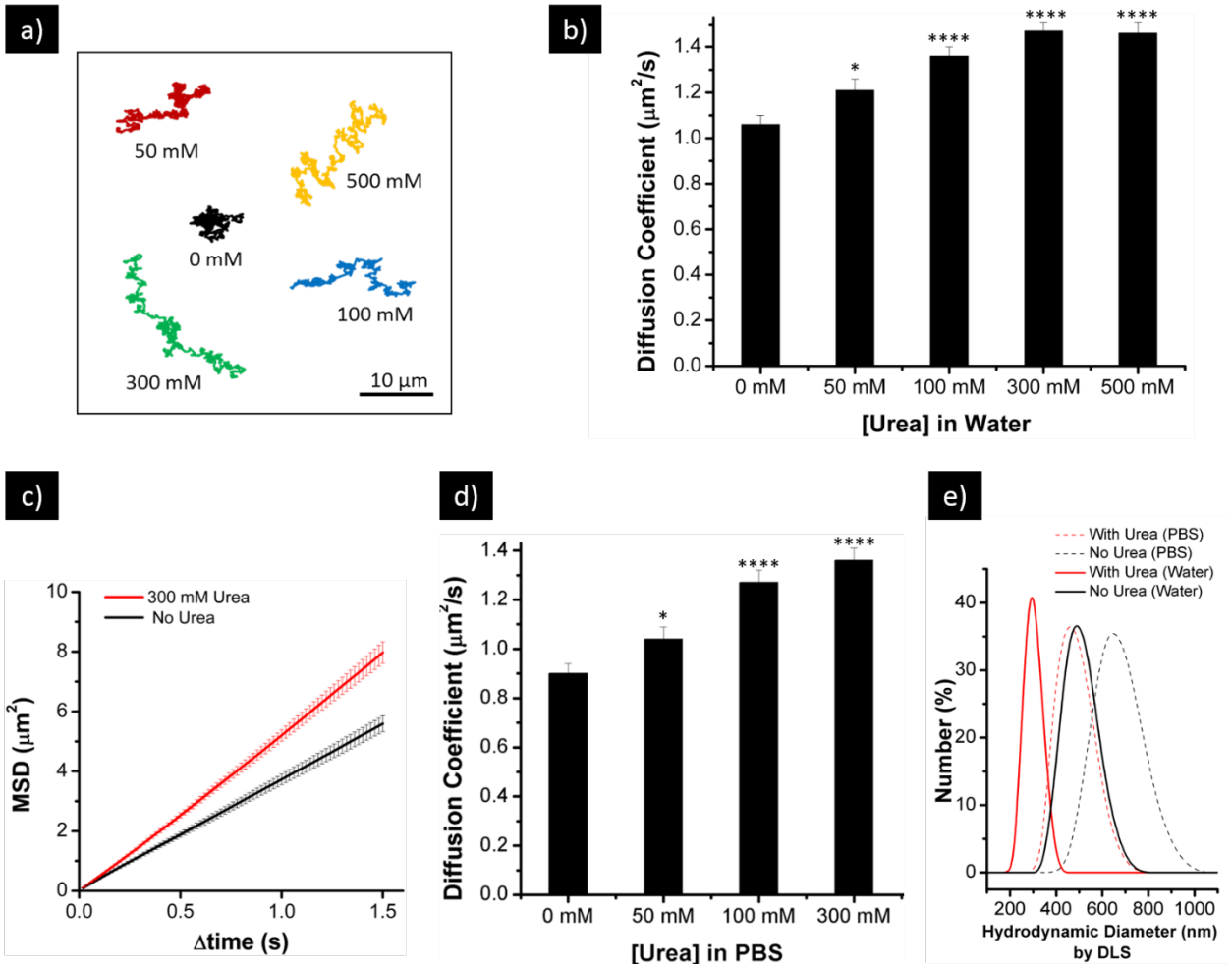

Figure 3. Analysis of the motion capability of the stimuli-responsive nanomotors (S1M). a) Representative tracking trajectories of the nanomotors during 15 s with different urea concentrations. b) Diffusion coefficient of nanomotors obtained by optical tracking at different urea concentrations (n=20, error bars represent s. e. m.). Superscripts denote statistically significant differences compared to diffusion at 0 mM of urea, with (*) $p<0.05$ and (****) $p<0.0001$ (ANOVA test). c) Mean square displacement (MSD) of nanomotors in PBS without and with urea (300 mM) in PBS (n=20, error bars represent s. e. m.). d) Diffusion coefficient in PBS (n=20, error bars represent s. e. m.). Superscripts indicate statistically significant differences compared to diffusion at 0 mM of urea, with (*) $p<0.05$ and (****) $p<0.0001$ (ANOVA test). e)

Apparent hydrodynamic diameter of nanomotors obtained by DLS without (black) and with urea (red, 300 mM) in water (continuous lines) and in PBS (dashed lines).

On-command controlled release studies.

Once demonstrated that the nanomotor **S1M** displays enhanced Brownian motion in the presence of urea, cargo release from **S1M** suspensions in different conditions was evaluated. In these experiments, **S1M** was brought to a concentration of 2.5 mg mL^{-1} in phosphate buffer at physiological pH (7.5) and at lysosomal pH (5). At scheduled times (each 20 min), aliquots were taken, centrifuged to sediment the nanoparticles and cargo release was determined by measuring $[Ru(bpy)_3]Cl_2$ absorbance in the supernatant. As can be observed in Figure 4a, at pH 7.5 the release was negligible after 100 min (ca. 2.5% of release efficiency), which indicates the correct capping of the material by the bulky cyclodextrin-modified urease. In contrast, a remarkable release occurred at pH 5 (ca. 20% of release efficiency), which could be appreciated even with the naked eye (Figure 4b). This was attributed to the protonation of benzimidazole groups ($pK_a = 5.5$)[59] and the subsequent rupture of the inclusion complexes between the protonated benzimidazole groups and β-cyclodextrin from the cyclodextrin-modified urease, which induced the dethreading of the caps allowing payload release.

In additional experiments, the amount of protein detached from **S1M** (corresponding to the CD-U caps) was quantified by the Bradford assay. No protein release was detected after **S1M** incubation at pH 7.5. In contrast, the amount of free protein in solution after **S1M** incubation at pH 5 was measured to be 145 μg mL^{-1}. On the other hand, release experiments with **S1** (without capping with CD-U) were also conducted. In this case, a marked cargo release from **S1** was observed at both physiological (7.5) and at lysosomal pH (5) (Figure SI-10), which confirms the advantage of blocking the pores with the cyclodextrin-modified urease for releasing the payload on-command.

Finally, we also evaluated whether the presence of the urea fuel induced any premature cargo leakage from **S1M** in buffer at neutral pH. For this, similar experiments to those explained above with **S1M** were carried out. Cargo delivery from **S1M** (concentration of 2.5 mg mL^{-1}) in phosphate buffer at pH 7.5 containing urea at a concentration of 100 mM was studied. The amount of cargo release was quantified from absorbance values, by applying Beer's-Lambert law, and the results are shown in Figure 4c. No significant cargo release was observed for **S1M** in media at neutral pH in the absence or presence of urea, which confirms the correct blockage of the pores in physiological buffer even in the presence of the fuel. In previous reports, non-gated catalytic nanomotors exhibited a large payload release in the presence of fuel due to motion. [15,32] This can produce the release of a non-negligible amount of cargo before reaching the target area/cells. In contrast, the gated nanomotors we report here do not show this effect, which can be an advantage for future therapeutic applications. Finally, we also tested the effect of urea in cargo delivery from **S1M** in media at pH 5, and found no significant difference between the amount released in the absence or presence of urea.

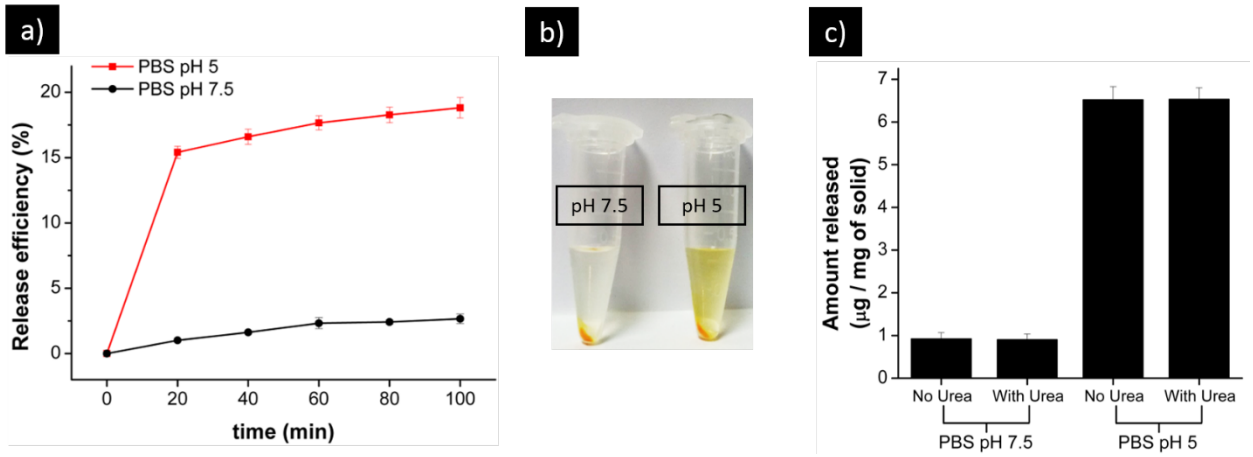

Figure 4. Cargo release experiments. a) Cargo release profile from stimuli-responsive nanomotors **S1M** in PBS at physiological pH (7.5, black curve) and at lysosomal pH (5, red curve). b) Visualization of $[Ru(bpy)_2]Cl_2$ released from **S1M** at pH 7.5 and at pH 5 to the solution, after

100 min of incubation. c) Amount of cargo released from **S1M** in PBS at pH 7.5 and at pH 5 in the absence and presence of urea (100 mM), quantified by measuring $[Ru(bpy)_2]Cl_2$ absorbance at 453 nm. Error bars represent s. e. m. from three independent experiments.

These *in vitro* studies demonstrated that (i) nanomotor **S1M** displays self-propulsion ability, (ii) no cargo delivery is observed in a competitive media such as phosphate buffer at physiological pH neither when the nanomotor is off (in the absence of urea) or on (in the presence of urea), and (iii) cargo delivery is triggered at acidic pH (simulating a lysosomal environment). Therefore, **S1M** fulfills some requirements of an ideal drug delivery vehicle and shows clear enhanced properties, in terms of autonomous mobility and controlled release, when compared with classical passive delivery systems.

Cargo delivery in cells.

Encouraged by the above mentioned results; i.e the selective delivery of the cargo (i.e $[Ru(bpy)_3]Cl_2$) at acidic pH and the enhanced Brownian motion showed by the nanomotor, we tested the short term cytotoxicity of **S1M** and cargo delivery, in the absence and the presence of urea, in human epithelial cervix adenocarcinoma HeLa cells. Short term cytotoxicity of the urea-powered gated **S1M** nanomotor was assessed by means of WST-1 cell viability assays (Figure 5). The data indicated that **S1M** did not affect cell viability at concentrations as high as 100 μg mL^{-1} in the absence of urea after the 24 h incubation period. In fact, a ca. 100% cell viability was found for the nanomotor in the 0-100 μg mL^{-1} concentration range, which covers the relevant concentrations recommended for the study of mesoporous silica nanoparticles toxitycity.[40] A very similar cell viability was observed in the presence of nanomotor and urea at a concentration of 50

mM indicating that neither, the biofuel urea, nor **S1M** with enhanced diffusion were toxic for HeLa cells. This urea concentration was selected to be in the range of that found in serum of patients suffering from conditions such as kidney disease, liver dysfunction, chemotherapy-induced renal damage or gastrointestinal problems.[60-62]

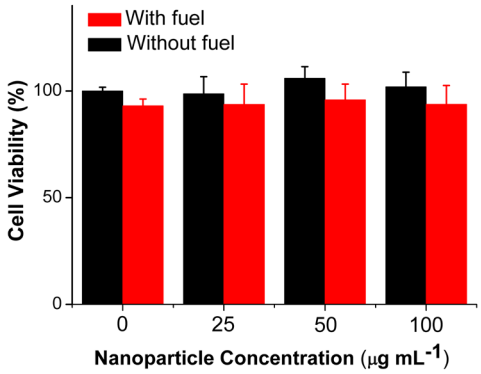

Figure 5. Cell viability. HeLa cell viability in the presence of nanomotors **S1M** at different concentrations in the absence and presence of urea (50 mM).

Internalization of **S1M** in HeLa cells in the absence and the presence of urea was studied by flow cytometry (FC). Despite the good performance of this technique,[63] its use to study the interaction of nanomotors with cells has not been previously reported. In these experiments, 50 μg mL^{-1} of **S1M** were added to the cell culture media in the absence or presence of urea (50 mM). At scheduled times, cells were injected in the FC instrument in order to measure cell fluorescence at 590 nm (which is associated to $[Ru(bpy)_3]Cl_2$, λ_{exc}=453 nm).

The FC results showed that the number of cargo-positive cells increased with time in both cases (in the presence and in the absence of the fuel), although a larger percentage of positive cells was found in the presence of urea (Figure 6a). For instance, after 5 minutes of incubation 32% of cargo-positive HeLa cells were found in the absence of urea, whereas this value increased to 48% in the

presence of the biofuel. Moreover, when the cargo intensity in cells was measured (which is related with the amount of **S1$_M$** internalized in cells), more evident differences with and without urea were found (Figure 6b). In fact, Figure 6b shows that the intensity of fluorescence in cells increased with time and that a remarkable larger intensity was found at any time (except at time zero) for the nanomotors incubated with urea. For instance, after 5 min of incubation, emission intensity at 590 nm was 2.7 times larger with urea when compared with the same results in the absence of the fuel (average fluorescence was 17751 without fuel and 47242 with fuel). After an incubation time of 60 min the intensity ratio in the absence and presence of urea was ca. 1.2 to 3 (average fluorescence was 37328 without fuel and 92398 with fuel). Representative cell population distributions (where the x-axis represents the emission of a cell and the y-axis represents the number of cells with that emission) obtained in a typical FC experiment are showed in Figure 6c, where the cells with a higher emission than the control (untreated cells) are determined as positive (red area). Additionally, we also prepared control nanoparticles (**S1$_{CD}$**) capped with β-cyclodextrin but lacking the enzyme and confirmed that in this case no enhancement in cell fluorescence was observed in the presence of urea (Figure SI-11). In further control experiments, we confirmed that the pH of the cell media remained buffered after incubation with nanomotors **S1$_M$** and urea. Moreover, the successful internalization of nanomotors in HeLa cells was confirmed by TEM (Figure SI-12) and by 3D confocal imaging (Figure SI-13).

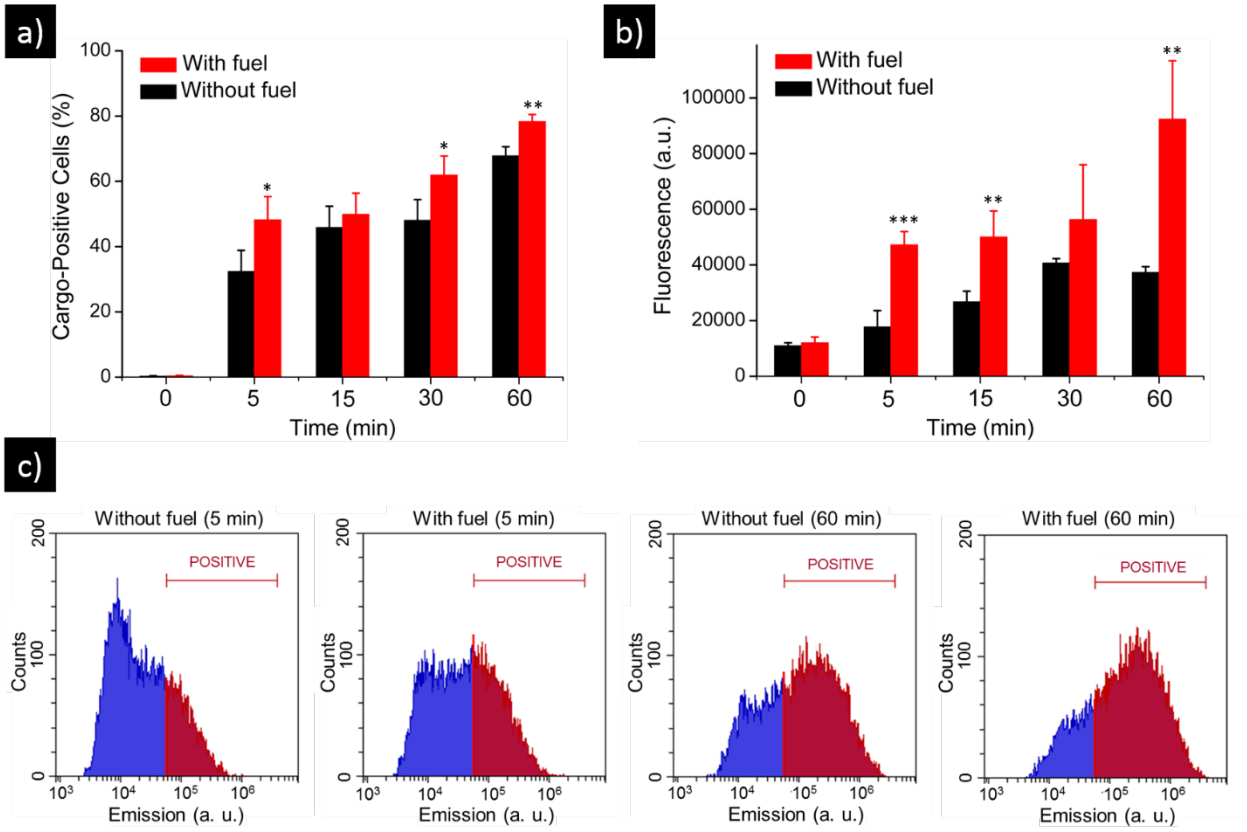

Figure 6. Flow cytometry studies. a) Analysis of the percentage of cargo-positive HeLa cells at different times. Cells were treated with 50 μg mL^{-1} of **S1M** in the absence and presence of urea (50 mM). Error bars represent s. e. m from three independent experiments. b) Analysis of $[Ru(bpy)_3]Cl_2$ associated-fluorescence of HeLa cells treated with 50 μg mL^{-1} of **S1M** in the absence and presence of urea (50 mM) at different times. Error bars represent s. e. m. from three independent experiments. Superscripts mark that the effect of fuel was statistically significant with (*) $p < 0.05$, (**) $p< 0.02$ and (***) $p< 0.001$, respectively. c) Representative population distributions (non-positive / cargo-positive cells) obtained in a typical flow cytometry experiment using the CytoFLEX S instrument after 5 min and 60 min.

In order to complete the studies showed above, we also prepared the nanomotors **S1MDOX**, which are similar to **S1M** but loaded with the drug doxorubicin (dox). The profiles of dox release can be

observed in Figure SI-14. In this case, the release efficiency of dox from **S1$_{MDOX}$** was 40% at pH 5, whereas it was negligible (only 1.6%) in phosphate buffer at neutral pH. Additionally, we confirmed that the particles remained capped (no dox was prematurely released) in cell culture media (DMEM supplemented with 10% FBS). To directly visualize intracellular cargo release, and since dox is fluorescent, we carried out experiments of **S1$_{MDOX}$** uptake by HeLa cells using confocal microscopy. For this, HeLa cells were incubated with 50 μg mL^{-1} of **S1$_{MDOX}$** for 1 hour in the absence and in the presence of urea (50 mM), and then washed to remove non-internalized nanoparticles. Cells were also stained with the DNA marker Hoechst 3342. Confocal images (Figure 7a) showed a clear increase in dox-associated fluorescence (λ_{exc}=480 nm, λ_{em}=550 nm) for cells treated with **S1$_{MDOX}$** incubated with the biofuel urea when compared with the control (absence of urea). A quantification of this increase in fluorescence was carried out using the *Image J* software to measure the emission inside cells. Double the fluorescence associated with dox was found for cells treated with nanomotor in the presence of urea (Figure 7b). These results (in terms of enhanced internalization and emission intensity) agree with those found in flow cytometry studies for **S1$_{M}$** (*vide ante*). As additional control experiments, we prepared dox-loaded nanoparticles **S2$_{DOX}$** (capped with β-cyclodextrin without urease) and confirmed that no increase in cell fluorescence was observe in the presence of urea (Figure 7a-b).

Finally, we also carried out studies of HeLa cell viability after treatment of HeLa cells with **S1$_{MDOX}$**. In the absence of fuel, a **S1$_{MDOX}$** concentration-dependent decrease of living cells was observed (cell viability was 54% at 25 μg mL^{-1} of **S1$_{MDOX}$**, 41% at 50 μg mL^{-1} and 35.2% at 100 μg mL^{-1}) (Figure 7c). In contrast, a larger cell viability reduction to about ca. 28% was observed when **S1$_{MDOX}$** was incubated with cells in the presence of urea (50 mM) even at nanomotor concentrations as low as 25 μg mL^{-1}. In fact, compared with the minimum of 35.2% viability in

the absence of fuel at a **S1$_{MDOX}$** concentration of 100 μg mL^{-1}, urea-fueled nanomotor produced even a larger viability decrease (to ca. 28% viability) using 4 times less nanoparticle concentration. Moreover, at the same nanoparticle concentration of 25 μg mL^{-1}, the presence of fuel resulted in a relative increase in cell death (reduction of cell viability) of 47% when compared with cells treated with **S1$_{MDOX}$** at the same concentration. From another point of view, taking into account that the total amount of dox in 25 μg mL^{-1} of **S1$_{MDOX}$** is 0.030 μM and that it reduces viability to 28% in the presence of fuel, the nanomotor has a considerably enhanced efficacy compared to free dox, since 0.374 μM of free dox has been reported to decrease HeLa cells viability to 50 %.[64]

Altogether, these results indicate that an enhanced cell uptake due to the enhanced Brownian motion of the nanomotor and a remarkable larger cargo release inside cells is observed, when urea is present in the medium. Note that, because of the design of the nanosystem, there is no cargo delivery in the cellular medium neither, in the absence nor in the presence of urea (Figure 4), yet cargo delivery only occurs after nanomotor internalization in cells due to the pH-triggered dethreading of the nanovalve.

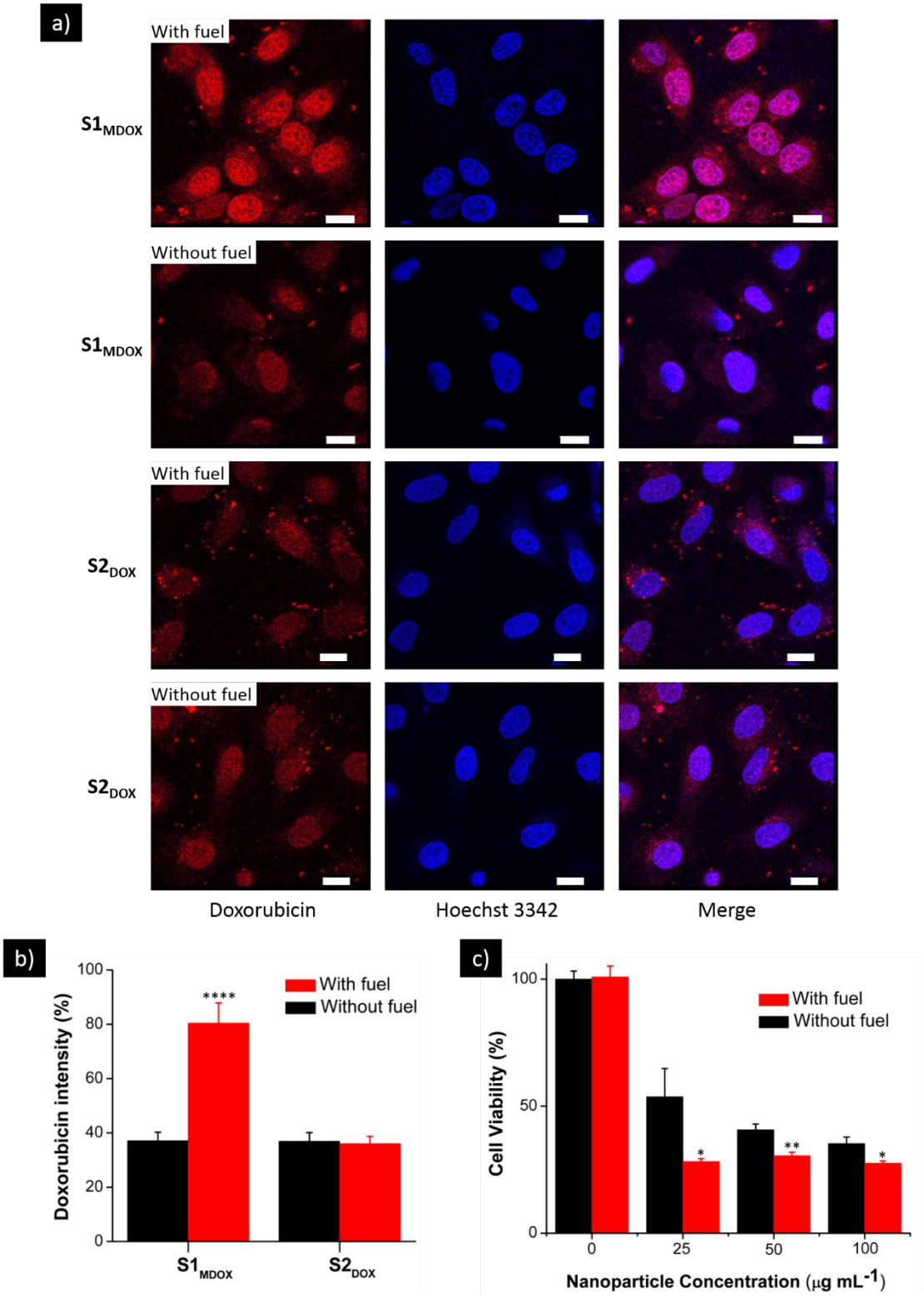

Figure 7. Delivery of doxorubicin in HeLa cells. a) Confocal microscopy images of HeLa cells treated with **S1MDOX** and with **S2DOX** (without urease) in the absence and presence of urea (50

mM). From left to right: doxorubicin fluorescence, DNA-marker (Hoechst 3342) fluorescence and combined (merge). Scale bars: 5 μm. b) Doxorubicin intensity quantification in cells from confocal images using the *Image J* software. c) Viability of HeLa cancer cells after 24 h of incubation with different concentrations of **S1$_{MDOX}$** in the absence and presence of urea (50 mM). Error bars represent s. e. m. from three independent experiments containing triplicates. Superscripts indicate statistically significant differences compared to absence of urea; with (*) $p<0.05$, (**) $p<0.005$ and (****) $p<0.0001$ (ANOVA test).

CONCLUSIONS

In summary, we report here the design, preparation and characterization of biocatalytic nanomotors based on mesoporous silica nanoparticles capped with supramolecular nanovalves for active cargo transport and pH-responsive release. In particular, mesoporous silica nanoparticles functionalized with benzimidazole groups and capped by the formation of inclusion complexes with cyclodextrin-modified urease (CD-U) were prepared. The nanomotor exhibits enhanced Brownian motion in the presence of urea thanks to enzymatic catalysis both, in water and in ionic media (PBS). At physiological pH, the supramolecular benzimidazole:CD-U nanovalve acts as a bulky stopper and prevents cargo release both in the absence and in the presence of urea. In contrast, a remarkable delivery occurs at lysosomal acidic pH due to protonation of benzimidazole groups and dethreading of the supramolecular ensemble. Experiments in cells show that the presence of the fuel enhances both nanomotors internalization and intracellular cargo delivery. This has been demonstrated for both, **S1$_{M}$** and **S1$_{MDOX}$**, loaded with the dye $[Ru(bpy)_3]Cl_2$ and doxorubicin, respectively. For the nanomotors loaded with doxorubicin, the presence of urea allowed to obtain a similar viability to that found in the absence of urea, but using 4 times less

nanoparticle concentration. Studies with the nanomotor loaded with $[Ru(bpy)_3]Cl_2$ demonstrated that the system has no short term cytotoxicity, a highly desired characteristic for biomedical applications. The improvement in drug delivery properties, in terms of enhanced effectiveness by gated enzyme-powered nanomotors, hold potential use in different biomedical settings, such as the active transport of a drug into a specific tissue or cell without drug leaking before reaching the target location, and payload delivery at-will using endogenous or exogenous stimuli. These findings may further motivate and inspire the development of novel micro- and nanomotors for the transport and stimuli-responsive controlled release of drugs.

METHODS

Chemicals. Tetraethylorthosilicate (TEOS, >99%), triethanolamine (TEOA, 99%), cetyltrimethylammonium bromide (CTAB, 99%), ethanol (>99%), hydrochloric acid (37%), (3-iodopropyl)trimethoxysilane (>95%), tris(2,2′-bipyridyl)dichlororuthenium(II) hexahydrate ($[Ru(bpy)_3]Cl_2$, benzimidazole (98%), triethylamine (TEA, 98%), sodium dihydrogen phosphate monohydrate (>99%), urease from *Canavalia ensiformis* (type IX), urea (99.9%), N-(3-dimethylaminopropyl)-NI-ethylcarbodiimide hydrochloride (EDC, >99%), N-hydroxysuccinimide (NHS, 98%), and urease activity assay kit were acquired from Sigma-Aldrich. Toluene (99%), acetonitrile (99.5%), disodium hydrogen phosphate heptahydrate (99%) were provided by Scharlau. Doxorubicin hydrochloride was purchased from Carbosynth. For cells experiments, Dulbecco's Phosphate Buffered Saline (PBS), Dulbecco's Modified Eagle's Medium (DMEM) - high glucose, Fetal Bovine Serum (FBS) were purchased from Sigma-Aldrich. Cell proliferation reagent WST-1 was obtained from Roche Applied Science (Madrid, Spain). All reagents were used as received.

Instruments. SEM images were acquired using a FEI NOVA NanoSEM 230 microscope working at 5 kV. TEM and STEM-EDX imaging was carried out using a JEOL JEM-2100 LaB6 electron microscope working at 200 kV accelerating voltage and equipped with an Oxford Instruments INCA x-sight (Si(Li) detector) and a Zeiss SESAM microscope (200 kV) equipped with an energy dispersive X-ray (EDX) spectroscopy system from ThermoFisher. PXRD measurements were performed on a Seifert 3000TT diffractometer using CuK_{α} radiation. N_2 adsorption-desorption isotherms were recorded on a Micromeritics TriStar II Plus automated analyzer. Zeta potential and hydrodynamic diameter experiments were performed with a ZetaSizer Nano ZS (Malvern). Elemental analysis was performed using a LECO CHNS-932 Elemental Analyzer. Enzymatic activity assay was carried out using an Infinite M200 PRO Multimode Microplate Reader. Optical videos were recorded using a Leica DMi8 inverted microscope equipped with a 63x water objective and a Hamamatsu Camera. Absorbance measurements were performed with a JASCO V-650 Spectrophotometer. Cell viability measurements were taken with a Wallac 1420 workstation. Flow cytometry studies were carried out using a CytoFLEX S instrument (Beckman-Coulter, USA). Confocal microscopy imaging was performed with a Leica TCS SP8 AOBS inverted laser scanning confocal microscope (Leica Microsystems Heidelberg GmbH).

Synthesis and characterization of β-cyclodextrin-modified urease (CD-U). β-cyclodextrin-modified urease (CD-U) was prepared following a procedure previously reported.[51,65,66] Briefly, a mixture of 10 mg of urease, 10 mg of EDC, 10 mg of NHS and 5 mg of aminated β-cyclodextrin in 2.5 mL of phosphate buffer (50 mM) was incubated for 24 h at 4 °C under stirring. After this, the modified enzyme was isolated by centrifugation using Amicon Ultra-05 centrifugal filter units with Ultracel-10 membranes, and dialyzed in phosphate buffer at pH 7.5. The resulting CD-U was

characterized by phenol-sulfuric acid method revealing a cyclodextrin content of 3 wt. % (see Supporting Information for details),[67] and by urease activity assay revealing an activity of 1.4 U mg^{-1}.

Synthesis of mesoporous silica nanoparticles (S0). CTAB (570 mg) and TEOA (35 g) were dissolved in a flask contain 20 mL of DI water. The mixture was subsequently heated in an oil bath at 95 °C for 30 min. Then, 1.5 mL of TEOS was added to the mixture dropwise. The reaction was allowed to proceed for 2 h under magnetic stirring. Then, the particles were collected and rinsed three times by centrifuging and redispersing in ethanol. To obtain the mesoporous structure, the as-prepared particles were dispersed in a solution containing 30 mL of methanol and 1.8 mL of HCl for 24 h reflux at 80 °C. Finally, the material was washed three times with ethanol and labelled as **S0**.

Preparation of S1. 100 mg of mesoporous nanoparticles (**S0**) were suspended in 8 mL acetonitrile containing 60 mg of $[Ru(bpy)_3]Cl_2$ and the mixture was stirred overnight. Then, 100 µL of (3-iodopropyl)trimethoxysilane were added and further stirred for 5.5 hours. Afterward, the solid was isolated by centrifugation, washed with acetonitrile and toluene, and let to dry at room temperature for 3 days. Next, we prepared a saturated solution of benzimidazole in toluene (500 mg in 30 mL of toluene mixed with 1485 µL of TEA and stirred for 20 min at 70 °C). 20 mL of this solution were added over the nanoparticles and the mixture was stirred for 3 days at 80 °C. Finally, the **S1** material was isolated by centrifugation, washed with toluene and acetonitrile, and dried at room temperature.

Preparation of $\mathbf{S1_M}$. 8 mg of **S1** and 3 mg of CD-U were stirred in 1 mL of sodium phosphate buffer overnight at 4 °C. Afterward, the capped material $\mathbf{S1_M}$ was exhaustively washed by

centrifugation with fresh buffer. The resulting material was kept refrigerated in phosphate buffer at a concentration of 10 mg mL^{-1} until use.

Optical video acquisition and MSD analysis. An aqueous solution of nanomotors **S1M** (0.02 mg mL^{-1}) was placed on a glass slide containing an aqueous solution of urea at the desired concentration. Then, a cover slip was used to cover the mixture in order to avoid any drifting artefact. Bright field videos of 30 s were recorded using a Hamamatsu camera working at a frame rate of 50 fps. Tracking of the nanomotors was performed by using an in-house developed Python code. After obtaining the tracked trajectories with corresponding coordinates (x, y), MSD was calculated using the formula:

$$MSD(\Delta t) = < \left(r(t + \Delta t) - r(t)\right)^2 >,$$

where *r* is the position of nanomotor at the initial time, *t* represents time, Δt is the elapsed time and <·> represents the time and ensemble average. The diffusion coefficient (*D*) is obtained by fitting the data of 20 particles per condition to MSD = 4 *D* Δt, according to previous studies.[52,53]

Triggered release experiments. S1M stock was washed with deionized water at pH 7.5, divided into fractions and brought to a concentration of 2.5 mg mL^{-1} in sodium phosphate buffer (10 mM) adjusted at the corresponding pH (7.5 or 5). At scheduled times, aliquots were taken and centrifuged at 12000 rpm for 2 min to precipitate the nanoparticles. Then, the supernatant absorbance at 453 nm was measured using the spectrophotometer in order to evaluate $[Ru(bpy)_3]Cl_2$ release. From absorbance, amount of released cargo was directly calculated by applying the Beer-Lambert's law:

$$Absorbance\ (453\ nm) = \varepsilon_{453} \cdot L \cdot C$$

Where ε_{453} is the molar extinction of $[Ru(bpy)_3]Cl_2$ at 453 nm (14600 M^{-1} cm^{-1}), L is the optical path of the cuvette (1 cm), and C is $[Ru(bpy)_3]Cl_2$ concentration. Furthermore, the maximum

release efficiency was calculated by treating the solid with 20% NaOH for 1 h, which dissolved the silica scaffold.

Cell culture conditions. HeLa human cervix adenocarcinoma cells were purchased from the German Resource Centre for Biological Materials (DSMZ) and were grown in DMEM supplemented with 10% FBS. Cells were incubated at 37 °C in an atmosphere of 5% carbon dioxide and 95% air and underwent passage twice a week.

Short term cytotoxicity studies. The short term cytotoxicity of the system was tested *in vitro* in the Hela cells. For this purpose, HeLa cells were seeded in a 96-well plate at 3500 cells/well and treated with different **S1M** concentrations (0, 25, 50, 100 μg mL^{-1}; we took aliquots from a stock of 2 mg mL^{-1} of **S1M** and added the corresponding amount to cell culture media in order to obtain the desired concentration) in the absence or presence of urea at 50 mM in the media. Cells were incubated for 24 h and the viability was determined by the WST-1 cell proliferation assay. Finally, absorbance was measured at 595 nm in the Wallac Workstation. Three independent experiments containing triplicates were carried out.

Internalization kinetics studies using flow cytometry. HeLa cells were seeded at 300.000 cells mL^{-1} in 6-well plate and incubated at 37 ºC for 24 h. Then, **S1M** was added at 50 μg mL^{-1} concentration in the absence or presence of urea (50 mM). At different times (0, 5, 15, 30 and 60 min), cells were washed with PBS to remove non-internalized nanoparticles, and collected for analysis by the cytometer. Three independent experiments were carried out.

TEM imaging of HeLa cells. Cell uptake of nanoparticles was confirmed by TEM. HeLa cells were seeded in chamber slides at 35000 cell/mL in DMEM (10% FBS) for 24h. Then, **S1M** was added to HeLa cell culture at 50μg mL^{-1}. After incubation, cells were washed and fixed with 3% of glutaraldehyde in sodium phosphate buffer (0.1 M), dehydrated in ethanol and stained with

uranyl acetate (1%) and osmium tetroxide (1%). The samples were included in epoxy resin (Araldite) and sectioned for TEM analysis. TEM images were acquired using a microscope FEI Tecnai Spirit G2 operating at 80kV with a digital camera (Soft Image System, Morada).

Confocal microscopy imaging of drug delivery. In order to test the potential use of enzyme-powered nanomotors equipped with pH-responsive nanovalves for the delivery of anticancer drugs, solid **S1$_{MDOX}$** was prepared (like **S1$_{M}$** but loaded with the cytotoxic drug doxorubicin). The amount of loaded doxorubicin was determined as 1.2 μmol per g of solid by UV-visible spectrophotometry. For visualization of doxorubicin delivery in a cancer cell line, HeLa cells were seeded over glass coverslips at 300.000 cells mL^{-1} in 6-well plate and incubated at 37°C for 24 h. Then, **S1$_{MDOX}$** was added to HeLa cell culture media at a concentration of 50 μg mL^{-1} in the absence or presence of urea (50 mM). After incubation for 1 h, cells were washed several times with PBS and finally, slides were visualized using a confocal microscope Leica TCS SP8 AOBS. Furthermore, the fluorescence intensity associated to doxorubicin was quantified using the Image J software.

Confirmation of S1$_{MDOX}$ internalization by 3D confocal imaging. HeLa cells were seeded in glass coverslips in 6-well plates at 350000 cells/mL in DMEM supplemented with 10% FBS for 24h. Then, **S1$_{MDOX}$** (50 μg mL^{-1}) was added and incubated for 1h. Afterwards, cells were washed and wheat germ agglutinin (5 μg mL^{-1}) and Hoechst 33342 (2 μg mL^{-1}) were added for confocal microscopy analysis. Serial optical slices were obtained of the samples from up to down (z-sections) to analyze the entirety of the cells and to confirm the nanoparticles uptake. Finally, the images were stacked creating a 3D reconstruction of the cell. Moreover, orthogonal sectioning was applied to determine the cellular localization of the nanoparticles.

Cell viability after treatment with $S1_{MDOX}$. For these experiments, HeLa cells were seeded in a 96-well plate at 3500 cells per well and treated with different and **$S1_{MDOX}$** concentrations (0, 25, 50 and 100 ug mL^{-1} in PBS) in the absence and in the presence of urea at 50 mM. Cells were incubated for 24h and the viability was determined by the WST-1 cell proliferation assay. Absorbance was measured at 595 nm in the Wallac Workstation. Three independent experiments containing triplicates were carried out.

Preparation of control nanoparticles without the urease enzyme. Control dye-loaded nanoparticles and control doxorubicin-loaded nanoparticles (lacking urease enzyme) were prepared by incubating 8 mg of the loaded solids with 1.2 mg mL^{-1} of β-cyclodextrin solution (without urease) overnight (sodium phosphate buffer, pH 7.5). Afterward, the capped materials were exhaustively washed with fresh buffer and isolated by centrifugation.

ASSOCIATED CONTENT

Supporting Information. Supporting figures (PDF) and videos (MP4).

AUTHOR INFORMATION

Corresponding Authors

*E-mail: rmaez@qim.upv.es

*E-mail: ssanchez@ibecbarcelona.eu

Author Contributions

The manuscript was written through contributions of all authors. All authors have given approval to the final version of the manuscript.

Notes

The authors declare no conflicts of interest.

ACKNOWLEDGMENTS

A. Llopis-Lorente is grateful to "La Caixa" Banking Foundation for his PhD grant. A. García-Fernández thanks the Spanish government for her FPU fellowship. The authors are grateful to the Spanish Government (MINECO Projects MAT2015-64139-C4-1, CTQ2014-58989-PCTQ2015-71936-REDT, CTQ2015-68879-R (MICRODIA) and CTQ2015-72471-EXP (Enzwim), the BBVA foundation (MEDIROBOTS)), the CERCA Programme by the Generalitat de Catalunya and the Generalitat Valencia (Project PROMETEO/2018/024 and PROMETEOII/2014/061) for support. TP thanks MINECO for the Juan de la Cierva post-doctoral fellowship. ACH thanks MINECO for the Severo Ochoa fellowship. The authors would like to thank A. Miguel-Lopez for the development of the python code for motion analysis.

REFERENCES

(1) Wang, J.; *Nanomachines: Fundamentals and Applications*; John Wiley & Sons, New York, **2013**.

(2) Mavroidis, C.; Ferreira, A. Nanorobotics: Current Approaches and Techniques; Springer, New York, **2013**.

(3) Wang, H.; Pumera, M. Fabrication of Micro/Nanoscale Motors. *Chem. Rev.* **2015**, *115*, 8704-8735.

(4) Li, J.; Esteban-Fernández de Ávila, B.; Gao, W.; Zhang, L. Wang, J. Micro/Nanorobots for Biomedicine: Delivery, Surgery, Sensing, and Detoxification. *Sci. Robot.* **2017**, *2*, eaam6431.

(5) Parmar, J.; Vilela, D.; Villa, K.; Wang, J.; Sánchez, S. Micro- and Nanomotors as Active Environmental Microcleaners and Sensors. *J. Am. Chem. Soc.* **2018**, *30*, 9317-9331.

(6) Xuan, M.; Wu, Z.; Shao, J.; Dai, L.; Si, T.; He, Q. Near Infrared Ligh-Powered Janus Mesoporous Silica Nanoparticle Motors. *J. Am. Chem. Soc.* **2016**, *20*, 6492-6497.

(7) Wang, J.; Xiong, Z.; Zheng, J.; Zhan, X.; Tang, J. Light-driven Micro/Nanomotors for Promising Biomedical Tools: Principle, Challenge and Prospect. *Acc. Chem. Res.* **2018**, *51*, 1957-1965.

(8) Chen, X. Z.; Hoop, M.; Mushtaq, F.; Siringil, E.; Hu, C.; Nelson, B. J.; Pané, S. Recent Developments in Magnetically Driven Micro- and Nanorobots. *Appl. Mater. Today* **2017***, 9*, 37-48.

(9) Xu, T.; Xu, L.-P.; Zhang, X. Ultrasound Propulsion of Micro-/Nanomotors. *Appl. Mater. Today* **2017***, 9*, 493-503.

(10) Dey, K. K.; Sen, A. Chemically Propelled Molecules and Machines. *J. Am. Chem. Soc.* **2017**, *139*, 7666-7676.

(11) Sánchez, S.; Soler, S.; Katuri, K. Chemically Powered Micro- and Nanomotors. *Angew. Chem. Int. Ed.* **2015**, *54*, 1414-1444.

(12) Peng, F.; Tu, Y.; Wilson, D. A. Micro/Nanomotors Towards *in vivo* Application. *Chem. Soc. Rev.* **2017***, 46,* 5289-5310.

(13) García-Gradilla, V.; Sattayasamitsathit, S.; Soto, F.; Kuralay, F.; Yardimci, C.; Wiitala, D.; Galarnyk, M.; Wang, J. Ultrasound-Propelled Nanoporous Gold Wire for Efficient Drug Loading and Release. *Small* **2014**, *10*, 4154-4159.

(14) Wu, Z.; Wu, Y.; He, W.; Lin, X. Sun, J.; He, Q. Self-Propelled Polymer-Based Multilayer Nanorockets for Transportation and Drug Release. *Angew. Chem. Int. Ed.* **2013**, *52*, 7000-7003.

(15) Ma, X.; Hahn, K.; Sánchez, S. Catalytic Mesoporous Janus Nanomotors for Active Cargo Delivery. *J. Am. Chem. Soc.* **2015**, 137, 4976-4979.

(16) Tu, Y.; Peng, F.; André, A. A. M.; Men, Y.; Srinivas, Y.; Wilson, D. A. Biodegradable Hybrid Stomatocyte Nanomotors for Drug Delivery. *ACS Nano* **2017**, *11*, 1957-1963.

(17) Tu, Y.; Peng, F.; White, P. B.; Wilson, D. A. Redox-Sensitive Stomatocyte Nanomotors: Destruction and Drug Release in the Presence of Glutathione. *Angew. Chem. Int. Ed.* **2017**, *56*, 7620-7624.

(18) Gao, W.; Pei, A.; Dong, R.; Wang, J. Catalytic Iridium-Based Janus Micromotors Powered by Ultralow Levels of Chemical Fuels. *J. Am. Chem. Soc.* **2014**, *136*, 2276-2279.

(19) Solovev, A. A.; Xi, W.; Gracias, D. H.; Harazim, S. M.; Deneke, C.; Sánchez, S.; Schmidt, O. G. Self-Propelled Nanotools. *ACS Nano* **2012**, *6*, 1751-1756.

(20) Dey, K. K; Zhao, X.; Tansi, B. M.; Méndez-Ortiz, W. J.; Córdova-Figueroa, U. M.; Golestian R.; Sen, A. Micromotors Powered by Enzyme Catalysis. *Nano Lett.* **2015**, *15*, 8311-8315.

(21) Patiño, T.; Arqué, X.; Mestre, R.; Palacios, L.; Sánchez, S. Fundamental Aspects of Enzyme-Powered Micro- and Nanoswimmers. *Acc. Chem. Res.* **2018**, *51*, 2662-2671.

(22) Zhao, X.; Gentile, K.; Mohajerani, F. Sen, A. Powering Motion with Enzymes. *Acc. Chem. Res.* **2018**, *51*, 2373-2381.

(23) Schattling, P. S.; Ramos-Docampo, M. A.; Salgueriño, V.; Städler, B. Double-Fueled Janus Swimmers with Magnetotactic Behaviour. *ACS Nano* **2017**, *11*, 3973-3983.

(24) Schattling, P. S.; Thingholm, B.; Städler, B. Enhanced Diffusion of Glucose-Fueled Janus Particles. *Chem. Mater.* **2015**, *27*, 7412-7418.

(25) Ma, X.; Wang, X.; Hahn, K.; Sánchez, S. Motion Control of Urea-Powered Biocompatible Hollow Microcapsules. *ACS* Nano **2016**, *10*, 3597-3605.

(26) Ma, X.; Hortelao, A. C.; Miguel-López, A.; Sánchez, S. Bubble-Free Propulsion of Ultrasmall Tubular Nanojets Powered by Biocatalytic Reactions. *J. Am. Chem. Soc.* **2016**, *138*, 13782-13785.

(27) Jang, W.-S.; Kim, J. H.; Gao, C.; Lee, D.; Hammer, D. A. Enzyme-Powered Surface-Associated Self-Motile Protocells. *Small* **2018**, *14*, 1801715.

(28) Simmchen, J.; Baeza, A.; Ruiz-Molina, D.; Vallet-Regí, M. Improving Catalase-Based Propelled Motor Endurance by Enzyme Encapsulation. *Nanoscale* **2014**, *6*, 8907-8913.

(29) Patiño, T.; Feiner-Gracia, N.; Arqué, X.; Miguel-López, A.; Jannasch, A.; Stumpp, T.; Schäffer, E., Albertazzi, L.; Sánchez, S. Influence of Enzyme Quantity and Distribution on the Self-Propulsion of Non-Janus Urease-Powered Micromotors. *J. Am. Chem. Soc.* **2018**, *140*, 7896-7903.

(30) Bunea, A.-I.; Pavel, I.-A.; David, S.; Gáspar, S. Sensing Based on the Motion of Enzyme-Modified Nanorods. *Biosens. Bioelectron.* **2015**, *67*, 42-48.

(31) Ma, X.; Jannasch, A.; Albrecht, U.-R.; Hahn, K.; Miguel-López, A.; Schäffer, E.; Sánchez, S. Enzyme-Powered Hollow Mesoporous Janus Nanomotors. *Nano Lett.* **2015**, *15*, 7043-7050.

(32) Hortelao, A. C.; Patiño, T.; Perez-Jiménez, A.; Blanco, A.; Sánchez, S. Enzyme-Powered Nanobots Enhance Anticancer Drug Delivery. *Adv. Funct. Mater.* **2017**, *28*, 1705086.

(33) Abdelmohsen, L. K. E. A.; Nijemeisland, M.; Pawar, G. M.; Janssen, G. E. A.; Nolte, R. J. M.; van Hest, J. C.; Wilson, D. A. Dynamic Loading and Unloading of Proteins in Polymeric Stomatocytes: Formation of an Enzyme-Loaded Supramolecular Nanomotor. *ACS Nano* **2016**, *10*, 2652-2660.

(34) Nijemeisland, M.; Abdelmohsen, L. K. E. A.; Huck, W. T. S.; Wilson, D. A.; van Hest, J. C. M. A Compartmentalized Out-of-Equilibrium Enzymatic Reaction Network for Sustained Autonomous Movement. *ACS Cent. Sci.* **2016**, *2*, 843-849.

(35) Wu, Z.; Lin, X.; Si, T.; He, Q. Recent Progress on Bioinspired Self-Propelled Micro/Nanomotors via Controlled Molecular Self-Assembly. *Small* **2016**, *23*, 3080-3093.

(36) Mura, S.; Nicolas, J.; Couvreur, P. Stimuli-Responsive Nanocarriers for Drug Delivery. *Nat. Mater.* **2013**, *12*, 991-1003.

(37) Llopis-Lorente, A.; de Luis, B.; García-Fernández, A.; Jimenez-Falcao, S.; Orzáez, M.; Sancenón, F.; Villalonga, R.; Martínez-Máñez, R. Hybrid Mesoporous Nanocarriers Act by Processing Logic Tasks: Toward the Design of Nanobots Capable of Reading Information from the Environment, *ACS Appl. Mater. Interfaces* **2018**, *10*, 26494-26500.

(38) Llopis-Lorente, A.; Díez, P; Sánchez, A.; Marcos, M. D.; Sancenón, F.; Martínez-Ruíz, P.; Villalonga, R.; Martínez-Máñez, R. Interactive Models of Communication at the Nanoscale Using Nanoparticles that Talk to One Another. *Nat. Commun.* **2017**, *8*, 15511.

(39) Croissant, J. G.; Fatieiev, Y.; Almalik, A.; Khashab, N. Mesoporous Silica and Organosilica Nanoparticles: Physical Chemistry, Biosafety, Delivery Strategies, and Biomedical Applications. *Adv. Healthcare Mater.* **2017**, *7*, 1700831.

(40) Tarn, D.; Ashley, C. E.; Xue, M.; Carnes, E. C.; Zink, J. I.; Brinker, C. J. Mesoporous Silica Nanoparticle Nanocarriers: Biofunctionality and Biocompatibility. *Acc. Chem. Res.* **2013**, *46*, 792-801.

(41) Coll, C.; Bernardos, A.; Martínez-Máñez, R.; Sancenón F. Gated Silica Mesoporous Supports for Controlled Release and Signaling Applications. *Acc. Chem. Res.* **2013**, *46*, 339-349.

(42) Wen, J.; Yang, K.; Liu, F.; Li, H., Xu, Y. Sun, S. Diverse Gatekeepers for Mesoporous Silica Nanoparticle Based Drug Delivery Systems. *Chem. Soc. Rev.* **2017**, *46*, 6024-6045.

(43) Aznar, E.; Oroval, M.; Pascual, L.; Murguía, J. R.; Martínez-Máñez, R.; Sancenón, F. Gated Materials for On-Command Release of Guest Molecules. *Chem. Rev.* **2016**, *116*, 561-718.

(44) Song, N.; Yang, Y.-W. Molecular and Supramolecular Switches on Mesoporous Silica Nanoparticles. *Chem. Soc. Rev.* **2015**, *44*, 3474-3504.

(45) Hernández-Montoto, A.; Montes, R.; Samadi, A.; Gorbe, M.; Terrés, J. M.; Cao-Milán, R.; Aznar, E.; Ibáñez, J.; Masot, R.; Marcos, M. D.; Orzáez, M.; Sancenón, F.; Oddershede, L. B.; Martínez-Máñez, R. Gold Nanostars Coated with Mesoporous Silica Are Effective and Nontoxic Photothermal Agents Capable of Gate Keeping and Laser-Induced Drug Release. *ACS Appl. Mater. Interfaces* **2018**, *10*, 27644-27656.

(46) de la Torre, C.; Casanova, I.; Acosta, G.; Coll, C.; Moreno, M. J.; Albericio, F.; Aznar, E.; Mangues, R.; Royo, M.; Sancenón, F.; Martínez-Mañez, R. Gated Mesoporous Silica Nanoparticles Using a Double-Role Circular Peptide for the Controlled and Target-Preferential Release of Doxorubicin in CXCR4-Expresing Lymphoma Cells. *Adv. Funct. Mater*. **2015**, *25*, 687-695.

(47) Agostini, A.; Mondragón, L.; Bernardos, A.; Martínez-Mañez, R.; Marcos, M. D.; Sancenón, F.; Soto, J.; Costero, A.; Manguan-García, C.; Perona, R.; Moreno-Torres, M.; Aparicio-Sanchis, R.; Murguía, J. R. Targeted Cargo Delivery in Senescent Cells Using Capped Mesoporous Silica Nanoparticles. *Angew. Chem. Int. Ed.* **2012**, *51*, 10556-10560.

(48) Climent, E.; Mondragón, L.; Martínez-Mañez, R.; Sancenón, F.; Marcos, M. D.; Murguía, J. R.; Amorós, P.; Rurack, K.; Pérez-Payá, E. Selective, Highly Sensitive, and Rapid Detection of Genomic DNA by Using Gated Materials: Mycoplasma Detection. *Angew. Chem. Int. Ed.* **2013**, *52*, 8938-8942.

(49) Ma, X.; Jang, S.; Popescu, M. N.; Uspal, W. E.; Miguel-López, A.; Hahn, K.; Kim, D.-P. Sánchez, S. Reversed Janus Micro/Nanomotors with Internal Chemical Engine. *ACS* Nano **2016**, *10*, 8751-8759.

(50) Xuan, M.; Shao, J.; Gao, C.; Wang, W.; Dai, L.; He, Q. Self-Propelled Nanomotors for Thermomechanically Percolating Cell Membranes. *Angew. Int. Ed.* **2018**, *57*, 12463-12467.

(51) Holzinger, M.; Bouffier, L.; Villalonga, R.; Cosnier, S. Adamantane/β-cyclodextrin Affinity Biosensors Based on Single-Walled Carbon Nanotubes. *Biosens. Bioelectron.* **2009**, *24*, 1128-1134.

(52) García-Fernández, A.; García-Laínez, G.; Ferrándiz, M. L.; Aznar, E.; Sancenón, F.; Alcaraz, M. J.; Murguía, J. R.; Marcos, M. D.; Martínez-Máñez, R.; Costero, A. M.; Orzáez, M. Targeting Inflammasome by the Inhibition of Caspase-1 Activity using Capped Mesoporous Silica Nanoparticles. *J. Control. Release* **2017**, *248*, 60-70.

(53) Brunauer, S.; Emmett, P. H.; Teller, E. Adsorption of Gases in Multimolecular Layers. *J. Am. Chem. Soc.* **1938**, *60*, 309-319.

(54) Barrett, E. P.; Joyner, L. G.; Halenda, P. P. The Determination of Pore Volume and Area Distributions in Porous Substances. I. Computations from Nitrogen Isotherms. *J. Am. Chem. Soc.* **1951**, *73*, 373-380.

(55) Bradford, M. A rapid and sensitive method for the quantitation of microgram quantities of protein utilizing the principle of protein-dye binding. *Anal. Chem.* **1976**, *72*, 248-254.

(56) Moliner-Martínez, Y.; Herráez-Hernández, R.; Campíns-Falcó, P. Improved Detection Limit for Ammonium/Ammonia Achieved by Berthelot's Reaction by Use of Solid-Phase Extraction Coupled to Diffuse Reflectance Spectroscopy. *Anal. Chim. Acta* **2005**, *534*, 327-334.

(57) Howse, J. R.; Jones, R. A. L.; Ryan, A. J.; Gough, T.; Vafabakshs, R.; Golestanian, R. Self-Motile Colloidal Particles: From Directed Propulsion to Random Walk. *Phys. Rew. Lett.* **2007**, *99*, 048102.

(58) Dunderlade, G.; Ebbens, S.; Fairclough, P.; Howse, J. Importance of Particle Tracking and Calculating the Mean-Squared Displacement in Distinguishing Nanopropulsion from Other Processes. *Langmuir* **2012**, *28*, 10997-11006.

(59) Jerez, G.; Kaufman, G.; Prystai, M.; Schenkeveld, S.; Donkor, K. K. Determination of Thermodynamic pK_a Values of Benzimidazole and Benzimidazole Derivatives by Capillary Electrophoresis. *J. Sep. Sci.* **2009**, *32*, 1087-1095.

(60) Pundir, C. S.; Jakhar, S.; Narwal, V. Determination of Urea with Special Emphasis on Biosensors: A Review. *Biosens. Bioelectron.* **2019**, *123*, 36-50.

(61) Ansari, S. G.; Wahab, R.; Ansari, Z. A.; Kim, Y.-S.; Khang, G.; Al-Hajry, A.; Shin, H.-S. Effect of Nanostructure on the urea sensing properties of sol-gel synthesized ZnO. *Sens. Actuators B* **2009**, *137*, 566-573.

(62) Guo, Y.; Wang, N.; Mou, J.; Zhao, Z.; Yang; J.; Zhu, F.; Pei, G.; Zhu, H.; Wang, Y.; Xu, G.; Yao, Y. Pretreatment of Huaiqihuang extractum protects against cisplatin-induced nephrotoxicity. *Sci. Rep.* **2018**, *8*, 7333.

(63) Ibrahim, S. F.; van den Engh, G. Flow Cytometry and Cell Sorting. *Adv. Biochem. Eng. Biotechnol.* **2007**, *106*, 19-39.

(64) Sadeghi-Aliabadi, H.; Minaiyan, M.; Dabestan, A. Cytotoxic Evaluation of Doxorubicin in Combination with Simvastatin against Human Cancer Cells. *Res. Pharm. Sci.* **2010**, *5*, 127-133.

(65) Aznar, E.; Villalonga, R.; Giménez, C.; Sancenón, F.; Marcos, M. D.; Martínez-Máñez, R.; Díez, P.; Pingarrón, J. M.; Amorós, P. Glucose-Triggered Release Using Enzyme-Gated Mesoporous Silica Nanoparticles. *Chem. Commun.* **2013**, *49*, 6391-6393.

(66) Oroval, M.; Díez, P.; Aznar, E.; Coll, C.; Marcos, M. D.; Villalonga, R.; Martínez-Máñez, R. Self-Regulated Glucose-Sensitive Neoglycoenzyme-Capped Mesoporous Silica Nanoparticles for Insulin Delivery. *Chem. Eur. J.* **2017**, *23*, 1353-1360.

(67) Dubois, M.; Gilles, K. A.; Hamilton, J. K.; Rebers, P. A.; Smith, F. Colorimetric Method for Determination of Sugars and Related Substances. *Anal. Chem.* **1956**, *28*, 350-356.